View metadata, citation and similar papers at core.ac.uk
brought to you by CORE
provided by MURAL - Maynooth University Research Archive Library

PHYSICAL REVIEW A **91**, 062306 (2015)

Optimizing for an arbitrary perfect entangler. I. Functionals

Paul Watts and Jiří Vala
Department of Mathematical Physics, National University of Ireland, Maynooth, Co. Kildare, Ireland
and School of Theoretical Physics, Dublin Institute for Advanced Studies, 10 Burlington Road, Dublin, Ireland

Matthias M. Müller and Tommaso Calarco
Institut für Quanteninformationsverarbeitung, Universität Ulm, 89081 Ulm, Germany

K. Birgitta Whaley
Department of Chemistry, University of California, Berkeley, California 94720, USA

Daniel M. Reich, Michael H. Goerz, and Christiane P. Koch
Theoretische Physik, Universität Kassel, Heinrich-Plett-Strasse 40, D-34132 Kassel, Germany
(Received 23 December 2014; published 8 June 2015)

Optimal control theory is a powerful tool for improving figures of merit in quantum information tasks. Finding the solution to any optimal control problem via numerical optimization depends crucially on the choice of the optimization functional. Here, we derive a functional that targets the full set of two-qubit perfect entanglers, gates capable of creating a maximally entangled state out of some initial product state. The functional depends on easily computable local invariants and unequivocally determines whether a gate is a perfect entangler. Optimization with our functional is most useful if the two-qubit dynamics allows for the implementation of more than one perfect entangler. We discuss the reachable set of perfect entanglers for a generic Hamiltonian that corresponds to several quantum information platforms of current interest.

DOI: 10.1103/PhysRevA.91.062306 PACS number(s): 03.67.Bg, 02.30.Yy

I. INTRODUCTION

Entanglement between quantum bits plays a fundamental role in quantum information processing. It is formed between two qubits by a suitable two-qubit operation from the Lie group SU(4). Physically, these operations correspond to the time evolution generated by some interaction Hamiltonian, or, in other words, by an element of the algebra su(4). Indeed, the question of optimally generating specific two-qubit operations became an important matter of quantum information and quantum control, as documented by several foundational works [1–5].

The starting point for our present study is the geometric theory of SU(4) that was formulated in Ref. [5]. It provides a classification of two-qubit operations in terms of their local equivalence classes. These are uniquely characterized by three real numbers known as local invariants [6]. Each local equivalence class contains all the two-qubit gates which are equivalent up to single-qubit transformations; it is characterized by a unique nonlocal content and thus has unique entangling capabilities.

The geometric theory has recently been combined with optimal control theory [7]. Specifically, using the local invariants which uniquely characterize local equivalence classes, the optimization target was expanded from a specific unitary operation to the corresponding local equivalence class. This considerably relaxes the control constraints. The ensuing optimization algorithm [7,8] allows for identifying those two-qubit gates out of a local equivalence class that can be implemented most easily for a given system Hamiltonian. The algorithm can be employed to determine the quantum speed limit [9], i.e., the fundamental limits for a given two-qubit system in terms of maximal fidelity and minimal gate time.

Here, we extend the definition of the optimization target from a local equivalence class to the full set of perfect entanglers (PEs) within the framework provided by the geometric theory [5]. Perfect entanglers are nonlocal two-qubit operations that are capable of creating a maximally entangled state out of some initial product state.

Our main result is twofold. We first formulate a function that uniquely identifies whether a two-qubit operation is a PE. We then incorporate this function into the optimal control functional that allows us to expand the optimization target to the full set of PEs. The optimization functional may be thought of as measuring the "minimal distance" between the gate U and the subset of matrices in SU(4) which are PEs. It is zero for a PE and positive otherwise. This function and thus the functional are given in terms of the local invariants; that is, they are remarkably easy to compute for any matrix, requiring only elementary algebra.

Numerical optimization proceeds by iteratively solving the control equations; each iteration yields a specific gate. Optimization targeting a local equivalence class (or a set of local equivalence classes) can therefore be visualized by a path in the Weyl chamber, i.e., the reduced two-qubit operation parameter space [7,8]. If the system dynamics using arbitrary controls allows for implementation of only a single local equivalence class containing a PE, the iterative "evolution" in the Weyl chamber is restricted to a line. However, our approach is most useful if more than one local equivalence class containing a PE can be reached. Optimization will then explore a larger portion of the Weyl chamber. We illustrate this with an analysis of the reachable set of local equivalence classes, considering a generic two-qubit Hamiltonian including controls that models superconducting qubits. The application of our optimization

 ©2015 American Physical Society

approach to specific physical examples is presented in the companion to this paper [10].

This paper is organized as follows. The geometric theory is summarized in Sec. II, with Sec. II A presenting a review of the way we decompose SU(4) to separate the purely local operations from the ones which entangle two qubits and Sec. II B reintroducing the set of easily computable numbers which are invariant under the local operations. Section III describes the subspace of the entangling gates which are PEs and introduces the functional that indicates when we have realized a PE. The reachable set of PEs for a generic two-qubit Hamiltonian is discussed in Sec. IV. Section V concludes.

II. REVIEW OF THE GEOMETRIC THEORY FOR TWO-QUBIT GATES

A. Decomposition and parametrization of SU(4)

All unitary gates operating on two-qubit states are described by a 4×4 unitary matrix, an element of the compact Lie group U(4). Any such matrix may be written as an element of SU(4) multiplied by a number of modulus 1, so the 16 parameters we use to specify any gate are the phase of this U(1) prefactor (an angle modulo 2π) and the 15 real parameters of SU(4).

Which 15 parameters we choose is largely up to us; the ones we use in this work are those arising from the Cartan decomposition of the Lie algebra of the group (cf. Ref. [11]). This decomposition allows us to write any element of SU(4) as a combination of two matrices in SU(2) $\otimes$ SU(2) and a matrix A [defined in Eq. (2) below] from the Cartan subgroup $\mathcal{A}$ whose Lie algebra is spanned by the maximal Abelian subalgebra of su(4) [5]. This decomposition is particularly suitable for applications such as optimal control [1].

The utility of this decomposition is apparent when we realize that, in the computational basis $\{|00\rangle,|01\rangle,|10\rangle,|11\rangle\}$, any operation which affects only the first qubit is represented by $U_1 \otimes I$, and one affecting only the second is $I \otimes U_2$, where U_1 and U_2 are each 2×2 unitary matrices. These *local* operations, which act separately and independently on the two qubits, are therefore described by matrices in SU(2) $\otimes$ SU(2). The operations which *entangle* the two qubits must then be entirely determined by the matrices from the Abelian subgroup $\mathcal{A}$. Gates are therefore denoted by equivalence classes living in $\mathcal{A}$; for example, [CNOT] is the set of gates which are equal to the CNOT (controlled-NOT) gate up to local operations.

With all of this in hand, we choose the decomposition of SU(4) such that our matrices take the form

$$U = k_1 A k_2 , \tag{1}$$

where k_1 and k_2 are 4×4 matrices in SU(2) $\otimes$ SU(2) and A is in the maximal Abelian subgroup $\mathcal{A}$. Twelve of the 15 coordinates necessary to specify any SU(4) element are included in k_1 and k_2. Since we work with gates in SU(4) modulo SU(2) $\otimes$ SU(2), we need use only the three coordinates c_1, c_2, and c_3, which parametrize the matrix A through

$$\begin{aligned} A &= \exp\left(-\frac{i}{2}\sum_{j=1}^{3} c_j \sigma_j \otimes \sigma_j\right) \\ &= \prod_{j=1}^{3}\left[I \otimes I \cos\left(\frac{c_j}{2}\right) - i\sigma_j \otimes \sigma_j \sin\left(\frac{c_j}{2}\right)\right], \end{aligned} \tag{2}$$

where $\sigma_{x,y,z}$ are the usual Pauli matrices. (Later in this article we shall use the shorthand $\sigma_i^{(1)} = \sigma_i \otimes I$ and $\sigma_i^{(2)} = I \otimes \sigma_i$.) To ensure that each U is given by a unique set of coordinates, we must restrict c_1, c_2, and c_3 to the Weyl chamber W given by

$$0 \leqslant c_3 \leqslant c_2 \leqslant c_1 \leqslant \frac{\pi}{2}$$

or

$$\frac{\pi}{2} < c_1 < \pi, \quad 0 \leqslant c_3 \leqslant c_2 < \pi - c_1 ,$$

i.e., within the tetrahedron whose vertices are at (0,0,0), (π,0,0), ($\pi/2$,$\pi/2$,0), and ($\pi/2$,$\pi/2$,$\pi/2$) [5].

B. Local invariants

Although c_1, c_2, and c_3 are defined in a straightforward manner, actually determining their values for a general element of SU(4) can be difficult. Fortunately, there are three alternative

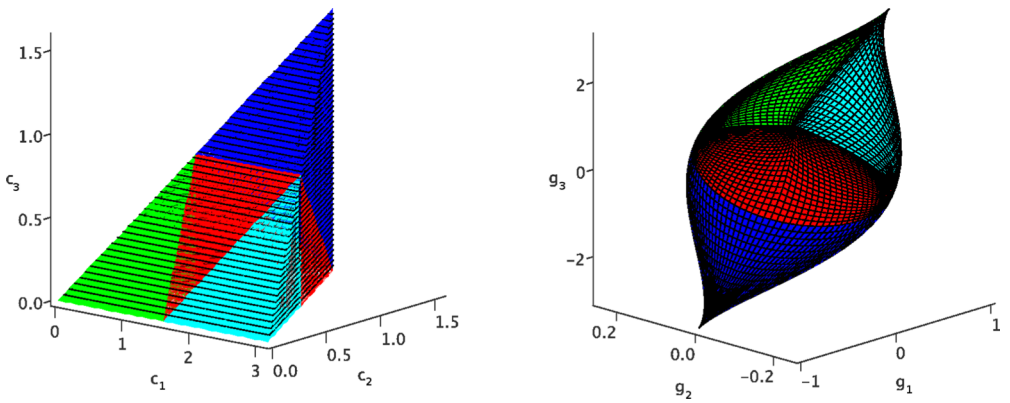

FIG. 1. (Color online) (left) The Weyl chamber in $c_1c_2c_3$ space and (right) its embedding in $g_1g_2g_3$ space. In both plots, W_0 is in green, W_0^* is in cyan, W_1 is in blue, and W_{PE} is in red. (The contours shown are purely for illustrative purpose.)

parameters which can be used as coordinates for local equivalence classes on $\mathcal{A}$ which are far easier to obtain.

If we change from the standard computational basis $\{|00\rangle,|01\rangle,|10\rangle,|11\rangle\}$ to a Bell basis given by

$$\left\{+\tfrac{1}{\sqrt{2}}(|00\rangle - i|11\rangle)\ ,\ -\tfrac{1}{\sqrt{2}}(i|01\rangle - |10\rangle),\right.$$
$$\left.-\tfrac{1}{\sqrt{2}}(i|01\rangle + |10\rangle)\ ,\ +\tfrac{1}{\sqrt{2}}(|00\rangle + i|11\rangle)\right\},$$

then our SU(4) matrices become $U_{\rm B} = Q^\dagger U Q = Q^\dagger k_1 A k_2 Q$, where

$$Q = \frac{1}{\sqrt{2}}\begin{pmatrix} 1 & 0 & 0 & i \\ 0 & i & 1 & 0 \\ 0 & i & -1 & 0 \\ 1 & 0 & 0 & -i \end{pmatrix}.$$

The eigenvalues of the matrix $m = U_{\rm B}^{\rm T} U_{\rm B}$ determine the local invariants of U [6]. The characteristic equation of m is

$$\lambda^4 - {\rm tr}(m)\lambda^3 + \tfrac{1}{2}[{\rm tr}^2(m) - {\rm tr}(m^2)]\lambda^2 - {\rm tr}^*(m)\lambda + 1 = 0,$$

so ${\rm tr}(m)$ and ${\rm tr}(m^2)$ give the local invariants. These are complex numbers. Instead, we may take as local invariants the three real numbers

$$g_1 = \tfrac{1}{16}{\rm Re}\{{\rm tr}^2(m)\}, \quad g_2 = \tfrac{1}{16}{\rm Im}\{{\rm tr}^2(m)\}\,,$$
$$g_3 = \tfrac{1}{4}[{\rm tr}^2(m) - {\rm tr}(m^2)].$$

Since m, m^2, and their traces are readily computable using the simplest of matrix operations, values for g_1, g_2, and g_3 can be easily obtained for any $U \in {\rm SU}(4)$.

Since g_1, g_2, g_3 are local invariants, they must be functions of only c_1, c_2, and c_3; some computation shows that they are, and they have the explicit forms

$$g_1 = \tfrac{1}{4}[\cos(2c_1) + \cos(2c_2) + \cos(2c_3) + \cos(2c_1)\cos(2c_2)\cos(2c_3)]\,,$$
$$g_2 = \tfrac{1}{4}\sin(2c_1)\sin(2c_2)\sin(2c_3)\,,$$
$$g_3 = \cos(2c_1) + \cos(2c_2) + \cos(2c_3).$$

These can be used to embed the tetrahedron defining the Weyl chamber into $g_1g_2g_3$ space; both spaces are shown in Fig. 1, with cross sections shown in Fig. 2. The coordinates of the local equivalence classes of some gates of interest are given in Table I.

TABLE I. Weyl coordinates c_1, c_2, c_3 of selected local equivalence classes [5] and their corresponding local invariants, g_1, g_2, g_3. DCNOT denotes double CNOT.

Equivalence class	c_1	c_2	c_3	g_1	g_2	g_3
[$\mathbb{1}$]	$0, \pi$	0	0	1	0	3
[DCNOT]	$\pi/2$	$\pi/2$	0	0	0	-1
[SWAP]	$\pi/2$	$\pi/2$	$\pi/2$	-1	0	-3
[B gate]	$\pi/2$	$\pi/4$	0	0	0	0
[CNOT]	$\pi/2$	0	0	0	0	1
[$\sqrt{\rm SWAP}$]	$\pi/4$	$\pi/4$	$\pi/4$	0	1/4	0

A particular combination which is quite useful is $\sqrt{g_1^2 + g_2^2}$; a quick calculation shows that

$$g_1^2 + g_2^2 = \tfrac{1}{16}[1 + \cos(2c_1)\cos(2c_2) + \cos(2c_1)\cos(2c_3) + \cos(2c_2)\cos(2c_3)]^2.$$

It is straightforward to confirm that the quantity inside the square brackets is always non-negative inside the Weyl chamber, so

$$\sqrt{g_1^2 + g_2^2} = \tfrac{1}{4}[1 + \cos(2c_1)\cos(2c_2) + \cos(2c_1)\cos(2c_3) + \cos(2c_2)\cos(2c_3)].$$

III. A FUNCTIONAL FOR PERFECT ENTANGLERS

In optimal control theory, the optimization functional measures how well the dynamics of the quantum system approaches a desired target. The target can be a specific final state [12], an entangled but otherwise arbitrary energy eigenstate [13], a specific unitary transformation for two or more qubits [14,15], a two-qubit local equivalence class [7], or another suitable measure of entanglement [16]. To be a suitable optimization functional, the figure of merit needs to fulfill two conditions: (i) It should take its optimum value if and only if the target is reached. (ii) It needs to be computable. For optimization algorithms that utilize gradient information,

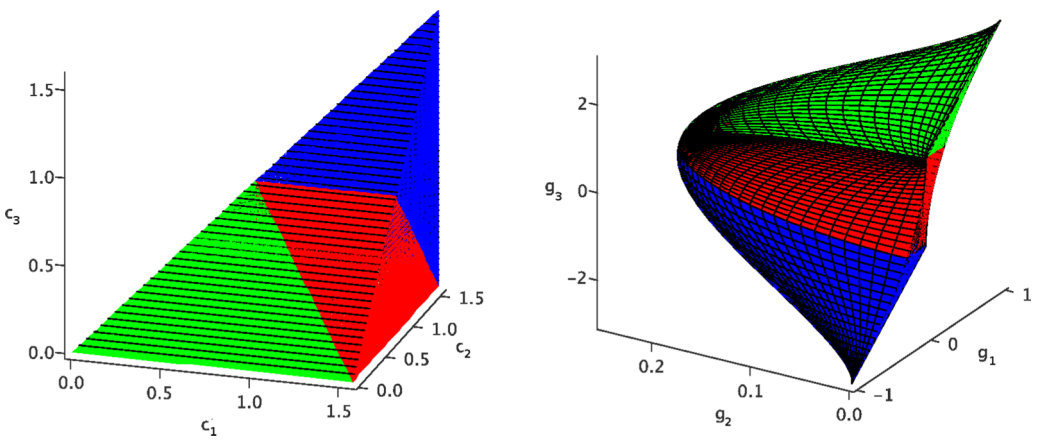

FIG. 2. (Color online) (left) The $0 \leqslant c_1 \leqslant \pi/2$ half of the Weyl chamber in $c_1c_2c_3$ space and (right) the corresponding $g_2 \geqslant 0$ half in $g_1g_2g_3$ space. In both cases, the full chamber is obtained by reflection across the cross section at the right of each plot.

the figure of merit in addition needs to be (almost everywhere) differentiable. Whatever the specific figure of merit is, its value depends on the system dynamics and thus on the unknown external control that drives the dynamics. It is therefore treated as a functional of the control. Note that due to the dependence of the optimization functional on the dynamics and the control, one needs to be able to compute the corresponding derivatives when evaluating the gradient [8,17].

Denoting the external control by $\epsilon(t)$, a possible target functional for a specific final state, for example, reads

$$F = |\langle\varphi_{\text{initial}}|U(T,0;\epsilon)|\varphi_{\text{target}}\rangle|^2 ;$$

that is, the figure of merit corresponds to the projection of the actual final state, $|\varphi(T)\rangle = U(T,0;\epsilon)|\varphi_{\text{initial}}\rangle$, onto the desired target state. Here, $U(T,0;\epsilon)$ denotes the unitary evolution that the system undergoes from time $t = 0$ to time $t = T$ under the control $\epsilon(t)$. For a specific unitary transformation, a suitable functional is given by [18]

$$F = \frac{1}{N}|\text{tr}(U^\dagger V)| ,$$

where V denotes the desired target operation, defined on a Hilbert space of dimension N, and U is again the actual system evolution. No matter which specific optimization method is employed, the target functional provides the information on the direction of the search, i.e., on how the control needs to be modified in order to improve the figure of merit.

In the following, we derive target functionals to optimize for an arbitrary perfect entangler. The idea is to quantify optimization success in terms of reaching a subset of SU(4), the subset of perfect entanglers, while the system evolution, in principle, can realize any element of SU(4) (or a subset thereof, depending on symmetries in the Hamiltonian). The quantification is achieved by a figure of merit that measures whether the actual system evolution U is a perfect entangler. The elements of SU(4) which perfectly entangle two-qubit states all lie within the subset of the Weyl chamber W bounded by the planes $c_1 + c_2 = \pi/2$, $c_1 - c_2 = \pi/2$ and $c_2 + c_3 = \pi/2$. This region is the seven-faced polyhedron with vertices at $(\pi/2,0,0)$, $(\pi/4,\pi/4,0)$, $(3\pi/4,\pi/4,0)$, $(\pi/2,\pi/2,0)$, $(\pi/4,\pi/4,\pi/4)$, and $(3\pi/4,\pi/4,\pi/4)$ [5]. W is thus divided up into four regions:

(1) W_{PE} is the perfect entanglers themselves.

(2) W_0 is the region between the origin (i.e., the identity element) and W_{PE}, the tetrahedron bounded by (but not including) the wall $c_1 + c_2 = \pi/2$. All three local invariants are positive in this region.

(3) W_0^*, between $(\pi,0,0)$ and W_{PE}, is bounded by $c_1 - c_2 = \pi/2$. In this region, g_1 and g_3 are positive and g_2 is negative. In fact, W_0^* can be obtained from W_0 via the transformation $(g_1,g_2,g_3) \to (g_1,-g_2,g_3)$.

(4) W_1, between W_{PE} and the [SWAP] gate at $(\pi/2,\pi/4,\pi/4)$, is bounded by $c_2 + c_3 = \pi/2$. g_1 and g_3 are both negative, and g_2 can have any sign.

One can construct functions based on a parametrization of W_{PE} either in terms of (c_1,c_2,c_3) or in terms of (g_1,g_2,g_3). In the following, we will refer to (c_1,c_2,c_3) as the Weyl coordinates and to (g_1,g_2,g_3) as the local invariants or Makhlin coordinates.

A. Gate fidelity for perfect entanglers in terms of the Weyl coordinates c_1, c_2, c_3

In order to define a fidelity for an arbitrary perfect entangler in terms of the Weyl coordinates c_1, c_2, c_3, we generalize the notion of the fidelity for a specific desired two-qubit gate V,

$$\tilde{F} = \tfrac{1}{4}|\text{tr}(U^\dagger V)| ,$$

where U is the actually implemented gate and we assume $U \in \text{SU}(4)$. Note that $\tilde{F}$ is a good approximation of the average gate fidelity [19], provided that U and V are not far from each other. This is sufficient to make it a suitable figure of merit for gate optimization. Allowing for complete freedom in the local transformations, we define our generalized figure of merit as

$$F = \max_{k_1,k_2 \in SU(2)\otimes SU(2)} \tfrac{1}{4}\text{Re}\{\text{tr}(U^\dagger k_1 V k_2^\dagger)\},$$

where we have substituted the modulus in $\tilde{F}$ by the real part. This approximation is justified when the equivalence classes $[U]$ and $[V]$ are close to each other. We further assume that all local transformations can be carried out easily and on a time scale much faster than the nonlocal transformations. The maximum over all local transformations k_1, k_2 is difficult to evaluate. However, the local transformations can be chosen such that U and V are given by their canonical forms $A_U = \exp[-i/2\sum_j c_j^U \sigma_j\sigma_j]$ and $A_V = \exp[-i/2\sum_j c_j^V \sigma_j\sigma_j]$. We denote this choice by $k_i = k_{i,U}k_{i,V}$. It can be shown that the partial derivatives of F with respect to the k_i vanish and that $F = 1$ for $U = V$. The latter simply follows from equality of the Weyl coordinates. The partial derivatives are obtained by parametrizing k_i as elements of $\text{SU}(2)\otimes\text{SU}(2)$ and the canonical forms of the nonlocal parts by c_1, c_2, c_3. This choice of the local transformations yields

$$\begin{aligned} F &= \tfrac{1}{4}\text{Re}\{\text{tr}(U^\dagger k_{1,U}k_{1,V}^\dagger V k_{2,V}^\dagger k_{2,U})\} \\ &= \tfrac{1}{4}\text{Re}\{\text{tr}(A_U^\dagger A_V)\} \\ &= \tfrac{1}{4}\text{Re}\{\text{tr}(Q^\dagger A_U^\dagger Q Q^\dagger A_V Q)\} \\ &= \tfrac{1}{4}\text{Re}\{\text{tr}(F_U^\dagger F_V)\}, \end{aligned}$$

with

$$\begin{aligned} F_U &= Q^\dagger A_U Q \\ &= \text{diag}(e^{-\imath\frac{c_1-c_2+c_3}{2}}, e^{-\imath\frac{c_1+c_2-c_3}{2}}, e^{-\imath\frac{-c_1-c_2-c_3}{2}}, e^{-\imath\frac{-c_1+c_2+c_3}{2}}) \\ &= \text{diag}(e^{-\imath\phi_{1,U}}, e^{-\imath\phi_{2,U}}, e^{-\imath\phi_{3,U}}, e^{-\imath\phi_{4,U}}) \end{aligned}$$

and $F_V = Q^\dagger A_V Q$, respectively. Inserting the explicit forms of F_U and F_V, we obtain

$$\begin{aligned} F &= \frac{1}{4}\text{Re}\{\text{tr}(F_U^\dagger F_V)\} = \frac{1}{4}\sum_{j=1}^{4}\cos(\varphi_{j,U} - \varphi_{j,V}) \\ &= \frac{1}{4}\Bigg(\cos\frac{\Delta c_1 - \Delta c_2 + \Delta c_3}{2} + \cos\frac{\Delta c_1 + \Delta c_2 - \Delta c_3}{2} \\ &\quad + \cos\frac{\Delta c_1 + \Delta c_2 + \Delta c_3}{2} + \cos\frac{\Delta c_1 - \Delta c_2 - \Delta c_3}{2}\Bigg) \\ &= \cos\frac{\Delta c_1}{2}\cos\frac{\Delta c_2}{2}\cos\frac{\Delta c_3}{2} \approx 1 - \frac{|\Delta\vec{c}|^2}{8} , \end{aligned} \tag{3}$$

where $\Delta c_i = c_{U,i} - c_{V,i}$. In order to find the closest perfect entangler V for a given gate U, we have to maximize the fidelity given by Eq. (3) with respect to $c_{V,i}$. To this end, we can exploit the fact that the sectors W_0, W_0^*, W_1 are separated from the polyhedron W_{PE} by three planes, and U is a perfect entangler if and only if

$$c_1 + c_2 \geqslant \frac{\pi}{2}, \quad c_1 - c_2 \leqslant \frac{\pi}{2}, \quad c_2 + c_3 \leqslant \frac{\pi}{2}.$$

If U lies in the polyhedron of perfect entanglers, we can simply choose $V = U$ and arrive at perfect fidelity $F = 1$. If $U \in W_0$, we have $c_1 + c_2 \leqslant \frac{\pi}{2}$, and the closest perfect entangler in terms of both fidelity and distance of the Weyl coordinates is given by the projection of U onto the wall, i.e., $c_{V,1} = \frac{\pi}{4} + \frac{c_{U,1}-c_{U,2}}{2}$, $c_{V,2} = \frac{\pi}{4} + \frac{c_{U,2}-c_{U,1}}{2}$, and $c_{V,3} = c_{U,3}$. The distance vector between U and V as a function of the Weyl coordinates is then given by

$$\Delta\vec{c} = \left(\frac{c_{U,1}+c_{U,2}}{2} - \frac{\pi}{4}, \frac{c_{U,1}+c_{U,2}}{2} - \frac{\pi}{4}, 0\right).$$

With the analogous approach for W_0^* and W_1 and using Eq. (3), we arrive at

$$F_{\mathrm{PE}}(U) = \begin{cases} \cos^2 \frac{c_{U,1}+c_{U,2}-\frac{\pi}{2}}{4}, & c_1 + c_2 \leqslant \frac{\pi}{2}, \\ \cos^2 \frac{c_{U,2}+c_{U,3}-\frac{\pi}{2}}{4}, & c_2 + c_3 \geqslant \frac{\pi}{2}, \\ \cos^2 \frac{c_{U,1}-c_{U,2}-\frac{\pi}{2}}{4}, & c_1 - c_2 \geqslant \frac{\pi}{2}, \\ 1 & \text{otherwise (inside } W_{\mathrm{PE}}). \end{cases} \tag{4}$$

As desired, this fidelity is a function of $c_{U,i}$; it equals 1 if and only if U is a perfect entangler and is smaller than 1 otherwise. $F_{\mathrm{PE}}(U)$ can be used as an optimization functional for algorithms which only evaluate the functional and do not in addition use gradient information. The latter would require analytic gradients with respect to the dynamics [8,17]. These cannot be obtained for $F_{\mathrm{PE}}(U)$ since there is no closed expression of the Weyl coordinates (c_1,c_2,c_3) as functions of U.

Often, the dynamics may explore a Hilbert space that is larger than the logical subspace of the qubits. The evolution in the logical subspace may then correspond to a nonunitary gate $\tilde{U}$. Employing a singular value decomposition of $\tilde{U}$ and renormalizing the singular values, a unitary approximation U of $\tilde{U}$ is obtained [7]. This allows us to utilize the same ideas that have led to the fidelity F_{PE} defined above. The two-qubit gate fidelity F becomes

$$F = \tfrac{1}{4}|\mathrm{tr}(\tilde{U}^\dagger V)|,$$

where $V = k_{1,U} A_V k_{2,U}^\dagger$ and A_V is the canonical form of the perfect entangler closest to the unitary approximation U, as measured by the distance in Weyl coordinates. In order to avoid explicit calculation of the two $k_{i,U}$ (which would have to be done in every iteration step of an optimization algorithm), we find the lower bound on the fidelity,

$$\begin{aligned} F &= \tfrac{1}{4}|\mathrm{tr}(\tilde{U}^\dagger V)| = \tfrac{1}{4}\mathrm{Re}\{\mathrm{tr}(\tilde{U}^\dagger V)\} \\ &= \tfrac{1}{4}\mathrm{Re}\{\mathrm{tr}(U^\dagger V)\} + \tfrac{1}{4}\mathrm{Re}\{\mathrm{tr}[(\tilde{U}-U)^\dagger V]\} \\ &\geqslant \tfrac{1}{4}\mathrm{Re}\{\mathrm{tr}(U^\dagger V)\} - \left|\tfrac{1}{4}\mathrm{tr}[(\tilde{U}-U)^\dagger V]\right| \\ &\geqslant F_{\mathrm{PE}}(U) - ||\tilde{U}-U||, \end{aligned}$$

where we have first used the choice of V that makes the trace real and then used both the Cauchy-Schwarz inequality and $||V|| = 1$.

B. Perfect entanglers and the local invariants

For optimization algorithms that utilize gradient information it is necessary to express the functional in a way that allows for analytic expressions of the derivatives [8]. This is not the case if the functional is expressed in terms of the Weyl coordinates (c_1,c_2,c_3) [7]. We therefore seek to rewrite the boundaries of the polyhedron W_{PE} in terms of the local invariants (g_1,g_2,g_3).

Let us first look at the boundary with W_0: it is defined by the plane $c_1 + c_2 = \pi/2$, and along this wall, $\cos(2c_2) = -\cos(2c_1)$ and $\sin(2c_2) = \sin(2c_1)$. This means that the values of the local invariants on this wall depend only on c_1 and c_3 through

$$\begin{aligned} g_1 &= \tfrac{1}{4}\sin^2(2c_1)\cos(2c_3), \\ \sqrt{g_1^2 + g_2^2} &= \tfrac{1}{4}\sin^2(2c_1), \\ g_3 &= \cos(2c_3). \end{aligned}$$

We can eliminate c_1 and c_3 entirely from the above to give

$$g_3 = \begin{cases} \frac{g_1}{\sqrt{g_1^2+g_2^2}} & g_1 \neq 0 \text{ or } g_2 \neq 0, \\ 1 & g_1 = g_2 = 0 \end{cases}$$

as the equation defining the PE boundary in terms of the local invariants. If we repeat this analysis for the walls separating W_0^* and W_1 from W_{PE}, we find that the *same* equation describes them all. So any U lying precisely on the boundary of W_{PE} has local invariants satisfying $g_3 = g_1/\sqrt{g_1^2 + g_2^2}$.

This suggests the definition of a function d which depends on an SU(4) matrix U via its local invariants and vanishes on the boundary of W_{PE}:

$$d(g_1,g_2,g_3) = g_3\sqrt{g_1^2 + g_2^2} - g_1. \tag{5}$$

This is not the only combination of the local invariants which vanishes on the boundary of W_{PE}; the reason we choose this particular definition of d comes from the fact that it is continuous for all values of g_1, g_2, and g_3. When we rewrite it in terms of the Weyl coordinates, we obtain the particularly simple form

$$\begin{aligned} d = \tfrac{1}{4}&[\cos(2c_1) + \cos(2c_2)][\cos(2c_1) + \cos(2c_3)] \\ &\times [\cos(2c_2) + \cos(2c_3)]. \end{aligned}$$

It is this form which allows us to see immediately that d is manifestly positive in W_0; thus, in terms of the local invariants, all points in W_0 satisfy $g_3\sqrt{g_1^2 + g_2^2} - g_1 > 0$. We noted above that W_0^* is simply the mirror reflection of W_0 since we may obtain it by changing the sign of g_2; thus, in reality, W_0 and W_0^* are not disconnected in terms of the local invariants but are joined along the $g_2 = 0$ plane. This is seen explicitly in Fig. 1, where $W_0 \cup W_0^*$ consists of the green and cyan regions of the Weyl chamber.

In g space, the boundary separating $W_0 \cup W_0^*$ from W_{PE} is a single continuous surface. To be precise, if we use cylindrical

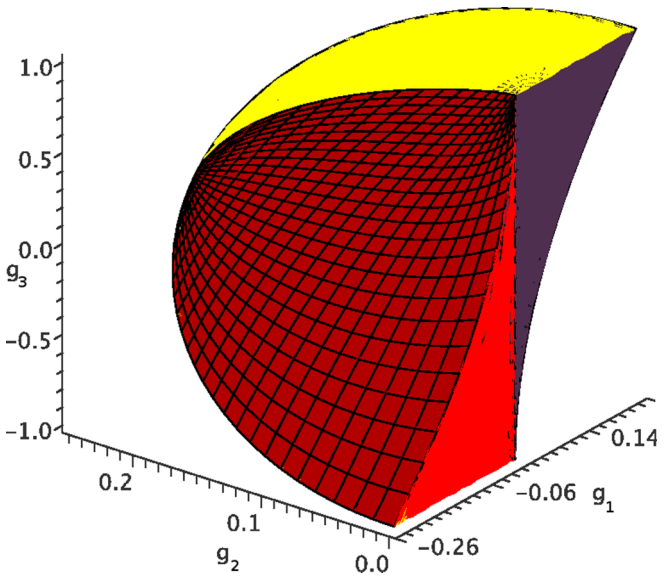

FIG. 3. (Color online) The $g_2 \geqslant 0$ half of the set of perfect entanglers W_{PE} in $g_1g_2g_3$ space. This space is divided into three regions: the red volume, where $d > 0$; the violet volume, where $d < 0$; and the surface composed of the boundary between them and the uppermost (yellow) and lowermost (obscured) surfaces, where $d = 0$.

coordinates (ρ,ϕ,z) defined by $g_1 = \rho\cos\phi$, $g_2 = \rho\sin\phi$, and $g_3 = z$, the boundary is given by the surface

$$z = \cos\phi, \quad -\frac{\pi}{2} \leqslant \phi \leqslant \frac{\pi}{2}, \quad \frac{1}{4}\sin^2\phi \leqslant \rho \leqslant \frac{1}{4}.$$

The part of this wall adjoining W_0 is the yellow surface illustrated in Fig. 3. As a result, if optimization starts from a gate U in $W_0 \cup W_0^*$, then $d(g_1,g_2,g_3) = g_3\sqrt{g_1^2+g_2^2} - g_1$ is an optimization function to reach a PE gate: we know that $d > 0$ for the initial gate and it reaches zero at the boundary with W_{PE}. However, d vanishes elsewhere as well: not only on the boundary between W_{PE} and W_1 but everywhere on the surface $z = \cos\phi$. This surface is composed of not only the boundaries that W_{PE} has with W_1 and $W_0 \cup W_0^*$ but also the boundary between the red and violet regions in Fig. 3. However, this surface lies entirely within W_{PE}, so the *only* gates U for which $d(g_1,g_2,g_3)$ vanishes are perfect entanglers.

However, d alone cannot tell us if we continue into the interior of W_{PE}. If U happens to cross the curve $z = \cos\phi$, $\rho = \sin^2\phi/4$, then either $d(g_1,g_2,g_3)$ becomes positive and we have a PE, or it becomes negative and we are in W_1 and do not have a PE. In either of these two cases, the value of d alone will not be a good enough indicator of whether we have evolved to a PE; further information might be necessary.

C. An optimization functional for perfect entanglers

The discussion of the previous two sections motivates our formulation of a functional $\mathcal{D}(U)$ that provides a *definitive* answer as to whether or not an SU(4) gate U is locally equivalent to a perfect entangler. That is, the functional vanishes if U is a perfect entangler and is positive otherwise.

The functional $\mathcal{D}(U)$ is based on the function $d(g_1,g_2,g_3)$ but also takes into account in which sector of the Weyl chamber, W_0, W_0^*, W_1, or W_{PE}, the local equivalence class of the gate U is located. Its construction is presented below:

(1) Compute the three Makhlin invariants g_1, g_2, and g_3 for U as usual.

(2) Next, find the three roots z_1, z_2, and z_3 of the cubic equation

$$z^3 - g_3z^2 + \left(4\sqrt{g_1^2+g_2^2} - 1\right)z + (g_3 - 4g_1) = 0$$

ordered such that $-1 \leqslant z_1 \leqslant z_2 \leqslant z_3 \leqslant 1$. These roots, which are functions of g_1, g_2, and g_3, facilitate the inverse map $(g_1,g_2,g_3) \to (c_1,c_2,c_3)$ and thus provide the location of the gate within the c-space Weyl chamber [20].

(3) Define d as in Eq. (5) and s as

$$s(g_1,g_2,g_3) = \pi - \cos^{-1} z_1 - \cos^{-1} z_3.$$

The definition of the functional $\mathcal{D}$ depends on the signs of these two functions:

(a) If d and s are both positive, then

$$\mathcal{D}(U) = g_3\sqrt{g_1^2+g_2^2} - g_1. \tag{6a}$$

(b) If d and s are both negative, then

$$\mathcal{D}(U) = g_1 - g_3\sqrt{g_1^2+g_2^2}. \tag{6b}$$

(c) In any other case,

$$\mathcal{D}(U) = 0. \tag{6c}$$

This gives the desired functional, one that is zero when the two-qubit gate is a perfect entangler and positive otherwise, with its value being a measure of how far the gate is from being a perfect entangler. Its evaluation requires only the Makhlin invariants and a way of finding the largest and smallest roots of a cubic equation. Since the Makhlin coordinates are straightforwardly expressed as functions of U (see Sec0 II B), analytic gradients of Eqs. (6a) and (6b) can be obtained. Therefore, $\mathcal{D}(U)$ represents an optimization functional that can be used with any optimization method, including those requiring analytic gradients [8,17].

IV. PERFECT ENTANGLER CONTROL IN THE WEYL CHAMBER

Optimization towards an arbitrary perfect entangler is most meaningful if the system dynamics allows the polyhedron of perfect entanglers to be approached from more than one direction or, more generally, for optimization paths in the Weyl chamber that explore more than one dimension. We therefore investigate the corresponding requirements on a generic two-qubit Hamiltonian,

$$H[u_1(t),u_2(t)] = \sum_{\alpha=1,2} \frac{\omega_\alpha}{2}\sigma_z^{(\alpha)} + u_1(t)\left(\sigma_x^{(1)} + \lambda\sigma_x^{(2)}\right) + u_2(t)\left(\sigma_x^{(1)}\sigma_x^{(2)} + \sigma_y^{(1)}\sigma_y^{(2)}\right). \tag{7}$$

Here, $\sigma_i^{(\alpha)}$ is the ith Pauli operator acting on the αth qubit of transition frequency ω_α, $u_1(t)$ is the single-qubit control field, where λ describes how strongly $u_1(t)$ couples to the

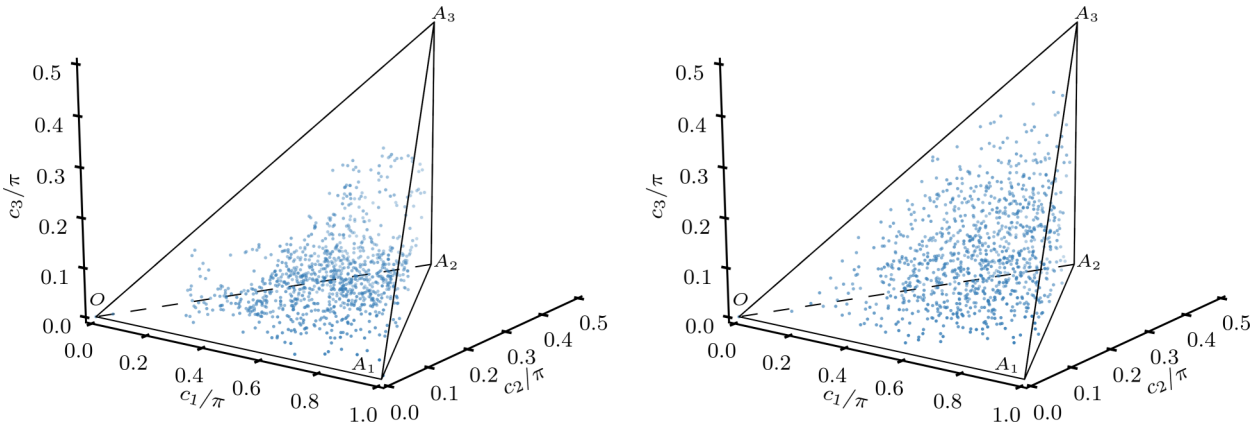

FIG. 4. (Color online) Sampling of reachable points in the Weyl chamber, obtained by solving Eq. (8) for the Hamiltonian (7) ($\lambda = 1$), a random pulse $u_1(t) \in [0,1]$, constant $u_2(t) \equiv 10^{-3}$, and 1000 time steps. (left) Result for $\omega_1 = 1.0 \neq \omega_2 = 1.1$, providing the full set of 15 generators in the Lie algebra. (right) Result for $\omega_1 = \omega_2 = 1$, providing nine generators. In both cases, every point in the Weyl chamber can be reached.

second qubit relative to the first one, and $u_2(t)$ is the two-qubit interaction control field. As discussed in more detail in the companion to this paper, Eq. (7) is often used to model qubits realized with superconducting circuits.

We analyze the solutions to the differential equation

$$\dot{U}(t) = -iH[u(t)]U(t), \quad U(0) = \mathbb{1} \tag{8}$$

for the unitary transformations U generated by the Hamiltonian (7). The reachable set of unitary transformations for a Hamiltonian is given in terms of the corresponding dynamical Lie algebra. It can be generated by taking the terms in (7) as a basis (neglecting orthonormalization for simplicity),

$$\sigma_z^{(1)}, \sigma_z^{(2)}, \sigma_x^{(1)} + \lambda\sigma_x^{(2)}, \sigma_x^{(1)}\sigma_x^{(2)} + \sigma_y^{(1)}\sigma_y^{(2)},$$

and constructing the repeated Lie brackets of these operators. This quickly yields all 15 canonical basis operators of SU(4), consisting of the single-qubit operators $\sigma_x^{(1)}$, $\sigma_x^{(2)}$, $\sigma_y^{(1)}$, $\sigma_y^{(2)}$, $\sigma_z^{(1)}$, and $\sigma_z^{(2)}$, as well as the entangling operators $\sigma_x^{(1)}\sigma_y^{(2)}$, $\sigma_y^{(1)}\sigma_x^{(2)}$, $\sigma_y^{(1)}\sigma_z^{(2)}$, $\sigma_z^{(1)}\sigma_y^{(2)}$, $\sigma_x^{(1)}\sigma_z^{(2)}$, $\sigma_z^{(1)}\sigma_x^{(2)}$, $\sigma_x^{(1)}\sigma_x^{(2)}$, $\sigma_y^{(1)}\sigma_y^{(2)}$, and $\sigma_z^{(1)}\sigma_z^{(2)}$. Hence, the system is completely controllable, and any point in the Weyl chamber can be reached.

The complete controllability is supported by the numerical solution of Eq. (8) for a random sequence of pulse values. The resulting gates are shown in the left panel of Fig. 4, and indicate full controllability since there are points in all regions of the Weyl chamber. Continuing the procedure to infinity would eventually fill the entire chamber. Neither setting $u_2(t)$ constant nor choosing $\lambda = 0$ places any restrictions on the controllability; indeed, it is sufficient if either the single-qubit terms or the interaction term can be controlled. While the controllability in this example was analyzed for arbitrary values of the parameters, the form of the Hamiltonian and the ratio between $\omega_{1,2}$ and u_2 fits the description of superconducting transmon qubits, with qubit energies in the gigahertz range and static qubit-qubit-coupling in the megahertz range.

Introducing symmetries in the Hamiltonian (7) reduces the controllability. First, we consider a situation in which the two qubits operate at the same frequency $\omega_1 = \omega_2$. In this case, the dynamic Lie algebra consists of only 9 instead of 15 operators. Consequently, not every two-qubit gate can be implemented. However, the nine operators include $\sigma_x^{(1)}\sigma_x^{(2)}$, $\sigma_y^{(1)}\sigma_y^{(2)}$, $\sigma_z^{(1)}\sigma_z^{(2)}$, which are sufficient to reach every point in the Weyl chamber [see Eq. (2)]. This is illustrated in the right panel of Fig. 4. Despite the reduced controllability, the Weyl chamber is more evenly filled after the same 1000 propagation steps as on the left. This counterintuitive finding is due to the lower dimension of the random walk, with no resources being "wasted" on the missing six single-qubit directions.

The set of gates that can be implemented with Hamiltonian (7) is more severely restricted if both qubits are completely degenerate, $\omega_1 = \omega_2 = 0$. This is typical for superconducting charge qubits operated at the "charge degeneracy point." Without any drift term, the Lie algebra consists of only four generators, $\sigma_z^{(1)}\sigma_y^{(2)} + \sigma_y^{(1)}\sigma_z^{(2)}$ and $\sigma_y^{(1)}\sigma_y^{(2)} - \sigma_z^{(1)}\sigma_z^{(2)}$ in addition to the two original terms. The implications for controllability in the Weyl chamber are not immediately obvious since three generators can be sufficient to obtain full Weyl chamber controllability. The easiest approach is to perform a numerical analysis, the results of which are shown on the left of Fig. 5. Two independent randomized pulses $u_1(t)$ and $u_2(t)$ were used. The reachable points lie on a plane, which due to the reflection symmetries appears as two triangular branches. Note that almost none of the common two-qubit gates are included in this set.

If only a single pulse is available to drive both the single-qubit and two-qubit terms, $u_1(t) \equiv u_2(t)$, and the qubits are degenerate, $\omega_1 = \omega_2 = 0$, there is a single generator for the dynamics. This situation is shown in the right panel of Fig. 5. Although there is only a single generator for the dynamics, a two-dimensional subset of the Weyl chamber can be reached. However, the subset is no longer the full plane as it is for two independent pulses (left panel of Fig. 5). Without single-qubit control, the center of the plane is no longer reachable. It is important to remember that while a single generator yields points on a line in the Weyl chamber (not necessarily a straight one), it can still fill an arbitrary subset of the Weyl chamber due to reflections at the boundaries. A similar example, restricted to the ground plane of the Weyl chamber, has been analyzed in Ref. [5].

Last, if there is no control over the individual qubits at all, $u_1(t) \equiv 0$, the only remaining generator is $\sigma_x^{(1)}\sigma_x^{(2)} + \sigma_y^{(1)}\sigma_y^{(2)}$.

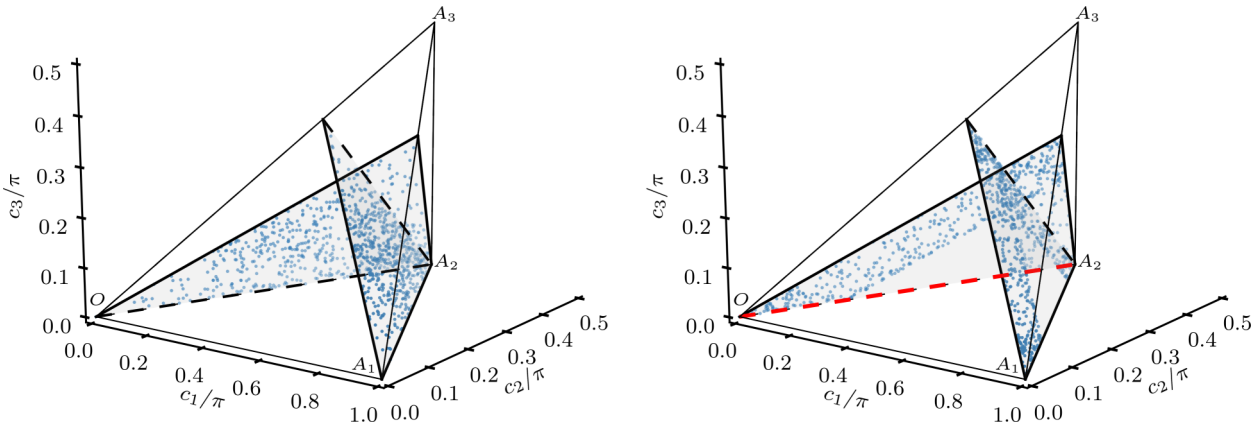

FIG. 5. (Color online) Same as Fig. 4 for the fully degenerate case $\omega_1 = \omega_2 = 0$ and two random pulses $u_1(t), u_2(t) \in [0,1]$. Not every point in the Weyl chamber can be reached. (left) For independent pulses $u_1(t)$, $u_2(t)$, the dynamic Lie algebra consists of four generators, and a two-dimensional subset of the Weyl chamber can be reached, indicated by the shaded triangles, O-$(\frac{2\pi}{3},\frac{\pi}{3},\frac{\pi}{3})$-$A_2$ and A_1-$(\frac{\pi}{3},\frac{\pi}{3},\frac{\pi}{3})$-$A_2$. (right) The reachable set is further reduced to a subset if $u_1(t) \equiv u_2(t)$, i.e., the single-qubit and interaction operators couple to the same pulse. Last, without single-qubit driving [$u_1(t) \equiv 0$], only a one-dimensional subset of the Weyl chamber can be reached, the red line O-A_2.

This corresponds to the straight line O-A_2 in the Weyl chamber, shown in red (gray) in Fig. 5. The line is reflected back onto itself at the A_2 point. Thus, in this case only a truly one-dimensional subset of reachable gates in the Weyl chamber can be realized.

For a Hamiltonian that allows for only a one-dimensional search space, optimal control calculations with a functional targeting all perfect entanglers will not yield results better than direct gate optimization. In contrast, for Hamiltonians allowing for two or three search directions in the Weyl chamber (see Figs. 4 and 5), the polyhedron of perfect entanglers may be approached from several different angles. Optimization with a functional targeting all perfect entanglers is then nontrivial. In such a search, the optimized solution will depend on additional constraints in the functional and the initial guess field. This will be explored in the companion to this paper.

V. SUMMARY

We have revisited the parametrization of two-qubit gates, i.e., elements of the Lie group SU(4), in terms of three real numbers, the local invariants [5], in order to derive an optimization functional for optimal control to target the whole subset of perfectly entangling two-qubit gates. We first identified an analytical function of the local invariants $d(g_1,g_2,g_3)$ which becomes zero at the boundary of the subset of perfect entanglers but can be of any sign within this subset. We rectified this ambiguity by using $d(g_1,g_2,g_3)$ to obtain a functional $\mathcal{D}(U)$ that determines definitively if we are within the set of perfect entanglers. Specifically, $\mathcal{D}(U)$ yields zero if a two-qubit gate U is a perfect entangler and is positive otherwise.

This functional represents a generalization of our earlier work on optimizing for a local equivalence class [7] instead of a specific gate [18]. Optimization with such a functional is useful if one wants to implement an arbitrary perfect entangler. In this case, a functional targeting the whole subset of perfect entanglers allows for more flexibility and thus potentially better control than optimization for a specific gate or a single local equivalence class. Furthermore, since gates locally equivalent to perfect entanglers occupy nearly 85% of SU(4) [20,21], the target of such a functional is very large indeed.

It is also conceivable to design an optimization functional targeting a set of two-qubit operations that is intermediate to a single local equivalence class and all perfect entanglers. For example, one could optimize for an arbitrary special perfect entangler which can maximally entangle a full product basis [22]. Such a functional can be obtained following the same design principles that we have outlined here. Similarly, it would be possible to maximize the entangling power of a two-qubit gate. The corresponding optimization functional is straightforward to write down since the entangling power is directly related to the local invariants g_1, g_2 [23].

While such generalized search strategies hold the promise of more flexibility and thus simpler searches, their full potential can be utilized only if the Hamiltonian is sufficiently complex, allowing us to approach the subset of perfect entanglers from more than one direction. For a generic two-qubit Hamiltonian, we have therefore analyzed the basic requirements for a nontrivial search. Not surprisingly, symmetries in the Hamiltonian preclude a full Weyl chamber search. Caution is necessary in particular when operating in the regime of the rotating-wave approximation, which typically introduces degeneracies and compromises complete controllability.

The companion to this paper illustrates optimization with the perfect entanglers' functional for several specific physical examples.

ACKNOWLEDGMENTS

We thank the Kavli Institute for Theoretical Physics for hospitality and for supporting this research in part by National Science Foundation Grant No. PHY11-25915. Financial support from the National Science Foundation under the Catalzying International Collaborations program (Grant No.

OISE-1158954), the Science Foundation Ireland under Principal Investigator Award No. 10/IN.1/I3013, the DAAD under Grant No. PPP USA 54367416, the European Commission through the EU-IP projects SIQS, DIADEMS, and RYSQ, as well as the coordination action QUAINT, and the DFG through SFB/TRR21 is gratefully acknowledged.

[1] N. Khaneja, R. Brockett, and S. J. Glaser, Phys. Rev. A **63**, 032308 (2001).
[2] C. H. Bennett, J. I. Cirac, M. S. Leifer, D. W. Leung, N. Linden, S. Popescu, and G. Vidal, Phys. Rev. A **66**, 012305 (2002).
[3] G. Vidal, K. Hammerer, and J. I. Cirac, Phys. Rev. Lett. **88**, 237902 (2002).
[4] K. Hammerer, G. Vidal, and J. I. Cirac, Phys. Rev. A **66**, 062321 (2002).
[5] J. Zhang, J. Vala, S. Sastry, and K. B. Whaley, Phys. Rev. A **67**, 042313 (2003).
[6] Y. Makhlin, Quantum Inf. Process. **1**, 243 (2002).
[7] M. M. Müller, D. M. Reich, M. Murphy, H. Yuan, J. Vala, K. B. Whaley, T. Calarco, and C. P. Koch, Phys. Rev. A **84**, 042315 (2011).
[8] D. M. Reich, M. Ndong, and C. P. Koch, J. Chem. Phys. **136**, 104103 (2012).
[9] T. Caneva, M. Murphy, T. Calarco, R. Fazio, S. Montangero, V. Giovannetti, and G. E. Santoro, Phys. Rev. Lett. **103**, 240501 (2009).
[10] M. H. Goerz, G. Gualdi, D. M. Reich, C. P. Koch, F. Motzoi, K. Birgitta Whaley, J. Vala, M. M. Müller, S. Montangero, and T. Calarco, Phys. Rev. A **91**, 062307 (2015).
[11] S. Helgason, *Differential Geometry, Lie Groups, and Symmetric Spaces* (Academic, New York, 1978).
[12] D. Tannor, V. Kazakov, and V. Orlov, in *Time-Dependent Quantum Molecular Dynamics*, edited by J. Broeckhove and L. Lathouwers (Plenum Press, New York, 1992), pp. 347–360.
[13] T. Caneva, T. Calarco, and S. Montangero, New J. Phys. **14**, 093041 (2012).
[14] J. P. Palao and R. Kosloff, Phys. Rev. Lett. **89**, 188301 (2002).
[15] C. M. Tesch and R. de Vivie-Riedle, Phys. Rev. Lett. **89**, 157901 (2002).
[16] F. Platzer, F. Mintert, and A. Buchleitner, Phys. Rev. Lett. **105**, 020501 (2010).
[17] N. Khaneja, T. Reiss, C. Kehlet, T. Schulte-Herbrüggen, and S. J. Glaser, J. Magn. Reson. **172**, 296 (2005).
[18] J. P. Palao and R. Kosloff, Phys. Rev. A **68**, 062308 (2003).
[19] L. H. Pedersen, N. M. Møller, and K. Mølmer, Phys. Lett. A **367**, 47 (2007).
[20] P. Watts, M. O'Connor, and J. Vala, Entropy **15**, 1963 (2013).
[21] M. Musz, M. Kuś, and K. Życzkowski, Phys. Rev. A **87**, 022111 (2013).
[22] A. T. Rezakhani, Phys. Rev. A **70**, 052313 (2004).
[23] S. Balakrishnan and R. Sankaranarayanan, Phys. Rev. A **82**, 034301 (2010).